



## Determination of porosity of lignocellulosic biomass before and after pretreatment by using Simons' stain and NMR techniques



Xianzhi Meng<sup>a</sup>, Marcus Foston<sup>a,1</sup>, Johannes Leisen<sup>b</sup>, Jaclyn DeMartini<sup>c</sup>, Charles E. Wyman<sup>c</sup>, Arthur J. Ragauskas<sup>a,\*</sup>

<sup>a</sup>BioEnergy Science Center, School of Chemistry and Biochemistry, Institute of Paper Science and Technology, Georgia Institute of Technology, 500 10th Street, Atlanta, GA 30332, USA

<sup>b</sup>School of Chemistry and Biochemistry, Georgia Institute of Technology, Atlanta, GA 30332, USA

<sup>c</sup>Department of Chemical & Environmental Engineering, Center for Environmental Research and Technology, University of California, Riverside, BioEnergy Science Center, Riverside, CA 92507, USA

### HIGHLIGHTS

- Cellulose accessibility was tested by Simons' stain and multiple NMR techniques.
- Pretreatment increases the pore size and overall surface area of the *Populus*.
- Different pretreatment effects cellulose accessibility to different extents.
- Pore expansion occurs primarily in first 10 min of the dilute acid pretreatment.

### ARTICLE INFO

#### Article history:

Received 13 April 2013

Received in revised form 23 June 2013

Accepted 24 June 2013

Available online 1 July 2013

#### Keywords:

Cellulose accessibility

Pretreatment

Simons' stain

NMR

Pore size distribution

### ABSTRACT

To further investigate the effect of dilute acid pretreatment (DAP) and steam explosion pretreatment (SE) on the change in cellulose accessibility, several techniques were applied including a Simons' stain (SS) technique along with several NMR methods (i.e., NMR cryoporometry, <sup>1</sup>H spin-lattice (T<sub>1</sub>) and <sup>1</sup>H spin-spin (T<sub>2</sub>) relaxometry, and diffusometry). These methods were utilized to probe biomass porosity and thus assess cellulose accessibility on untreated and pretreated *Populus*. In general, these techniques indicate that pretreated *Populus* has larger pore size distributions and specific surface area (SSA) when compared to an untreated sample. The SS method revealed that DAP is more effective than SE in terms of the SSA increase, and that DAP increases SSA as a function of pretreatment severity. Relaxometry and diffusion measurements also suggest pore expansion occurs primarily in the first 10 min of DAP.

© 2013 Elsevier Ltd. All rights reserved.

### 1. Introduction

The demand for renewable fuel sources continues to grow, in part due to the diminishing supply of fossil fuel resources as well as growing concerns about environmental stewardship and energy security. Lignocellulosic biomass, composed of cellulose, hemicellulose, and lignin, is one of the most abundant potential sustainable sources for renewable fuel production (Ragauskas et al., 2006). Undoubtedly, biofuels derived from this renewable resource, biomass, will play a key role in reducing the world dependence on fossil fuels. Bioconversion of lignocellulose is significantly hindered by the innate recalcitrance of biomass. As a result, achieving reasonable conversion rate and yield profiles necessitates the

inclusion of a pretreatment stage. Commonly cited goals of pretreatment, which is usually done prior to enzymatic deconstruction of cellulose, are (1) to remove/redistribute hemicellulose/lignin, (2) to disrupt the ultrastructure of cellulose, and (3) to open the lignin and hemicellulose matrix encapsulating cellulose, ultimately increasing the proportion of enzyme accessible surface area (Pu et al., 2008). Dilute acid and steam explosion pretreatment are two of the leading technologies that have seen significant research efforts over the past few decades. This research has been conducted in the areas of pretreatment optimization and scale-up; however, for significant future improvements to occur, an improved understanding of the fundamentals of biomass recalcitrance must be obtained.

Lignocellulosic substrate characteristics, e.g., crystallinity, degree of polymerization, specific surface area (SSA), and lignin/hemicellulose distribution, have been all thought to influence the efficiency of enzymatic hydrolysis (Mansfield et al., 1999). The porosity of lignocellulosic biomass or the SSA of exposed cellulose

\* Corresponding author. Tel.: +1 404 894 9701; fax: +1 404 894 4778.

E-mail address: [arthur.ragauskas@chemistry.gatech.edu](mailto:arthur.ragauskas@chemistry.gatech.edu) (A.J. Ragauskas).

<sup>1</sup> Current address: Department of Energy, Environmental & Chemical Engineering, Washington University, 1 Brookings Drive, St. Louis, MO 63130, USA.

in lignocellulosic biomass has been identified as a particularly important factor in influencing enzymatic deconstruction rate and yield. This dependence between cellulose accessibility and enzymatic deconstruction is associated with intimate contact between cellulose and cellulases such as exo-1,4- $\beta$ -D-glucanase, as a prerequisite step for enzymatic hydrolysis to occur. Some research on the relationship between biomass pore size and enzymatic hydrolysis suggest that small pores (i.e., those with diameters smaller than the diameters of cellulase enzymes) hinder and large pores enhance enzymatic hydrolysis (Tanaka et al., 1988). In the case of small pores, only small cellulase components can diffuse slowly inside the pores and consequently may become trapped there, causing a (1) decrease in molecular movement, (2) decrease in synergistic interaction, and (3) ultimately lower the rate of cellulose deconstruction. However, when large pores dominate the biomass pore system, the probability that the entire enzyme will have access and that synergistic catalytic action will occur becomes so high that the influence of the diffusion inside small pores becomes negligible and subsequently that the enzymatic hydrolysis yield and rate becomes significant (Foston and Ragauskas, 2010). This was supported by the fact that the initial rate of hydrolysis of steam pretreated mixed hardwood, poplar and white pine is linearly correlated with the pore volume of the substrate accessible to a nominal diameter of 5.1 nm representative of the size of the cellulase from *Trichoderma reesei* (Grethlein, 1985). This is also consistent with the fact that if cellulases are approximately spherical, they were from 2.4 to 7.7 nm in diameter, with a mean of 5.9 nm (Tanaka et al., 1988).

Historically, considerable amounts of work have been done in developing accessible surface area measurement techniques performed on cellulosic substrates, including electron microscopy (White and Brown, 1981), gas (e.g., nitrogen or water) adsorption (Chen et al., 2010), and mercury porosimetry (Simitzis et al., 1995). However, most of these techniques require a prior drying of the substrate which makes it typically less effective in determining the pore volume due to the fact that water removal from non-rigid porous materials could produce partial irreversible collapse of pores (Choudhary et al., 2012). Other techniques such as solute exclusion, can measure the substrate in its wet state, but it requires significant experiment time and it only measures the interior surface of the cellulose (Wang et al., 2012). In addition, gas adsorption methods typically result in an over-estimation of cellulose accessibility due to the fact that the molecular size of the probe gas is much smaller than cellulase enzymes. For all these reasons, the best techniques for surface area measurement are those (1) that can be directly applied to wet materials, and (2) that measure the overall surface area in a relative short time. Most of the current studies only use one technique for evaluating biomass accessibility. However, it is our opinion that this is inadequate, different techniques are based on different principles of measurement and their results reflect different physical measurement associated with accessibility, consequently, utilizing only one method will often provide incomplete information, and accounts for conflicting result or data interpretation.

In the present study, a modified Simons' stain (SS) method along with several NMR techniques was utilized to measure the cellulose accessibility/porosity of various pretreated *Populus* samples. The pretreatment techniques used in this study include dilute acid pretreatment (DAP) and steam explosion (SE). Using calculated dye adsorption, cryoporometry pore size distribution (PSD) curves, nuclear relaxation time distributions, and diffusion coefficient distributions, information about changes in the accessibility of lignocellulosic substrate upon pretreatment was resolved. This work was done in an effort (1) to generate a more accurate description of cellulose accessibility via multiple methods and (2) to further test the changes in the accessibility of lignocellulosic

substrate upon pretreatment, thus yielding a better understanding of the fundamentals of biomass recalcitrance.

## 2. Methods

### 2.1. Biomass feedstock

Baseline *Populus* (*Populus trichocarpa*  $\times$  *deltoides*) were harvested between 2007 and 2008 at Oak Ridge National Laboratory, TN. *Populus* is among the fastest-growing trees in North America and is well suited for a variety of applications such as biofuels production, pulp and paper, and other bio-based products, such as chemicals and adhesives. Samples were shipped to National Renewable Energy Laboratory (NREL) in Golden, CO for room temperature air drying, debarking, and size-reduction. Extractives were subsequently removed by adding ~5 g of biomass into an extraction thimble in a Soxhlet extraction apparatus. The extraction flask was filled with a 1:2 ethanol/benzene mixture and refluxed at a boiling rate which cycled the biomass for ~6 h.

### 2.2. Biomass pretreatment

For dilute acid pretreatment, lignocellulosic samples were first prepared by presoaking in a ~0.15 mol/L dilute sulfuric acid solution for 4 h at room temperature. The presoaked slurry was then filtered to remove the solid material and washed with an excess of deionized water. A mass of 3.00 g of the presoaked samples were transferred to a 300 mL mini-Parr reactor with ~0.15 mol/L sulfuric acid solution at 5% dry solids. The reactor was then sealed under ambient atmospheric conditions, and heated to 150 °C over ~30 min (~6 °C min<sup>-1</sup>). The Parr reactor was held at this temperature ( $\pm 2$  °C) for two specified residence time  $\pm 30$  s (10 min and 60 min), and then quenched in an ice bath for ~5 min. The pretreated slurry was filtered to remove the solid material and washed with an excess of deionized water. The steam explosion pretreatment was done at University of California, Riverside, and samples were used as received. Milled biomass was placed into a woven metal mesh basket, which was then suspended in a 4 L Hastelloy steam reactor. Steam for pretreatment was provided by a Fulton steam boiler (FB-075-L, Fulton Companies, Pulaski, NY), which was controlled by setting the boiler pressure to the saturated steam pressure corresponding to the target temperature of 150 °C. Pretreatments were performed at 150 °C for the specified reaction time, after which the temperature and pressure were suddenly dropped by opening a valve at the bottom of the vessel, discharging all pretreatment liquid. After cooling, the metal basket was removed from the steam reactor, and the pretreated milled biomass was recovered.

### 2.3. Chemical composition analysis

The chemical composition of each of the substrates was determined by the Klason protocol according to the TAPPI standard method T-222. In brief, the extractive-free samples were treated with 72% sulfuric acid for 4 h at 30 °C and then diluted to 3% sulfuric acid using deionized water and subsequently autoclaved at 121 °C for ~1 h. The resulting solution was cooled to room temperature and the precipitate was then filtered through a G8 glass fiber filter (Fisher Scientific, USA), dried, and weighed to get the Klason lignin content. The resulting filtrate was used for the detection of sugar composition by high-performance anion exchange chromatography with pulsed amperometric detection (HPAEC-PAD) using Dionex ICS-3000 (Dionex Corp., USA), and the acid-soluble lignin was measured by ultraviolet spectroscopy based on the TAPPI Method UM 250.

## 2.4. Dye preparation for Simons' stain

Direct Blue 1 (Pontamine Fast Sky Blue 6BX) and Direct Orange 15 (Pontamine Fast Orange 6RN) dyes were obtained from Pylam Products Co. Inc. (Garden City, NY). Direct Blue 1 was used as received. Although the original staining method developed by Simons utilized both the orange and blue dye as received (Simons, 1950), later studies suggested that only the high molecular weight fraction of the Direct Orange dye was responsible for the increased affinity for cellulose, whereas the low molecular weight part had a very similar affinity for cellulose as the Direct Blue dye did (Yu and Atalla 1998). Therefore an ultrafiltration of the orange dye to remove the low molecular weight part is necessary, and it is done by filtering a 1% solution of orange dye through a 100 K membrane using an Amicon ultrafiltration apparatus (Amicon Inc., Beverly, MA) under ~200 kPa nitrogen gas pressure (Esteghlalian et al., 2001).

## 2.5. Simons' stain

Fiber samples (~100 mg) were weighed into five centrifuge tubes, and 1.00 mL of phosphate buffered saline solution (pH 6, 0.3 M PO<sub>4</sub>, 1.40 M NaCl) was also added to each tube. A set of tubes containing 1:1 mixture of DB and DO dyes at increasing concentrations were prepared by adding same amount of DB and DO dyes in a series of increasing volumes (0.25, 0.5, 0.75, 1.00, 1.50 mL), which can be then used to measure the dye adsorption isotherm. Distilled water was added to each tube to make up the final volume to 10.00 mL. All these centrifuge tubes were incubated at 70 °C for ~6 h with shaking at 200 rpm. After that, the absorbance of the supernatant solution was obtained on a Lambda 35 UV-vis spectrophotometer at 455 nm and 624 nm which represent the wavelength of maximum absorbance for DO and DB, respectively.

## 2.6. Sample preparation for NMR experiments

*Populus* samples were never frozen but were stored at 4 °C prior to conditioning. Untreated and pretreated chips were conditioned in a sealed desiccator at 25 °C and ~100% relative humidity over a 0.01 (w/v) NaN<sub>3</sub> solution for 14 days. The moisture contents in all samples were found to be 60 ± 3%.

## 2.7. NMR experiments

### 2.7.1. Cryoporometry NMR experiments

The <sup>1</sup>H experiments were carried out in a Bruker static probe at frequencies of 300.13 MHz on a Bruker DSX-300 spectrometer. To completely remove all the possible ice signals, the <sup>1</sup>H NMR signals were collected using a standard Carr–Purcell–Meiboom–Gill sequence with a 5 μs (90°) <sup>1</sup>H pulse, 10 μs (180°) <sup>1</sup>H pulses, 16 scans, 10 s recycle delay, *n* = 8 echoes leading to an effective echo time of 0.00168 s prior to the acquisition of the FID. The hydrated sample was cooled to –50 °C slowly to completely freeze all the adsorbed water, and then the intensity of the NMR signal, which represents the amount of unfrozen water at a specific temperature, was recorded at intervals of 5 °C from –50 °C to –20 °C and then 1 °C from –20 °C to 0 °C. At each temperature increment, samples were allowed to equilibrate for 10–20 min. The signal intensities measured at each temperature (*T*) were corrected according to Curie's law under the assumption of a linearized Boltzmann distribution.

### 2.7.2. <sup>1</sup>H spin–spin (*T*<sub>2</sub>) NMR experiments

<sup>1</sup>H spin–spin (*T*<sub>2</sub>) NMR measurements were carried out in a Bruker static probe at frequencies of 300.13 MHz on a Bruker DSX-300 spectrometer. Experiments were conducted using the Bruker

Topspin software environment at a constant temperature of 25 °C. The spin–spin relaxation times were determined using a standard 2D Carr–Purcell–Meiboom–Gill (CPMG) sequence with a 5 μs (90°) <sup>1</sup>H pulse, 10 μs (180°) <sup>1</sup>H pulses, 16 scans, 10 s recycle delay and  $\tau = 0.0002$  s, 16 data points were recorded between *n* = 4 and 1024 echoes (0.00164–0.41984 s).

### 2.7.3. <sup>1</sup>H spin–lattice (*T*<sub>1</sub>) NMR experiments

<sup>1</sup>H spin–lattice (*T*<sub>1</sub>) NMR measurements were carried out in a Bruker static probe at frequencies of 300.13 MHz on a Bruker DSX-300 spectrometer. Experiments were conducted using the Bruker Topspin software environment at a constant temperature of 25 °C. The inversion recovery experiments utilized a 10 μs (90°) <sup>1</sup>H pulse, 10 μs (180°) <sup>1</sup>H pulse, 10 s recycle delay and 128 scans.

### 2.7.4. <sup>1</sup>H Diffusion NMR experiments

<sup>1</sup>H diffusion NMR measurements were carried out in the Bruker Micro-25 NMR accessories at frequencies of 400.13 MHz on a Bruker DSX-400 spectrometer. The radiofrequency coil used with this accessory had a diameter of 10 mm and an active length of about 30 mm. The *Populus* sample was placed inside a 10 mm NMR tube with the gradient-composition axis parallel to the long axis of the tube, and wet cotton in the cap to maintain a ~100% RH environment. Experiments were conducted using the XWINNMR software at a constant temperature of 25 °C. Diffusion coefficients were measured using a pulse field gradient (PFG) simulated echo sequence utilized a 10 μs (90°) <sup>1</sup>H pulse and 10 s recycle delay with 128 scans,  $\Delta = 25, 50, 100,$  and 200 ms, taking 64 points varying  $\delta$  between 0.0001 and 0.003 s.

Inverse Laplace transforms (ILT) were accomplished by a Matlab 7.13 program written at Victoria University of Wellington (Wellington, New Zealand) by P.T. Callaghan to process 1- and 2-dimensional ASCII data measuring either diffusion or relaxation characteristics of heterogeneous proton systems. This program is based on unconstrained regularization, non-negative least squared fit and singular value decomposition algorithms. The routine was tested using a series of multi-exponential and stretched-exponential functions of varying component weights, widths and characteristic decay times demonstrating fairly good accuracy, resolution and stability in the corresponding distributions produced. To assess the effect of noise, relaxation curves were generated using a multi-exponential function, and each data point was allowed to increase or decrease by a maximum of 10% of its only value. The particular variance at each data point was controlled by a random number generator to simulate a randomly noisy relaxation curve.

## 3. Results and discussion

### 3.1. Chemical composition analysis

The chemical composition of *Populus* including carbohydrate and lignin distribution before and after pretreatment is presented in Table 1, with glucose representing the major monosaccharide. The majority of the hemicellulose, typically characterized by xylose, mannose, arabinose, and galactose contents, was removed within 10 min of DAP. However, there are still significant amounts of xylose and mannose left in the *Populus* sample after 10 min SE pretreatment. In terms of acid insoluble lignin content, results indicate that both DAP and SE are ineffective at the removal of the majority of lignin, and the acid insoluble lignin content actually increases after dilute acid pretreatment possibly due to the formation of pseudo-lignin (Hu et al., 2012).

**Table 1**  
Chemical composition of untreated and pretreated *Populus*.

Substrate	Arabinan	Xylan	Glucan	Galactan	Mannan	AIL	ASL
Untreated <i>Populus</i>	0.3	11.5	50.3	0.6	1.9	34.7	0.5
10 min DAP <i>Populus</i>	0.0	3.5	58.1	0.0	0.1	36.9	0.6
60 min DAP <i>Populus</i>	0.0	0.2	56.5	0.0	0.2	42.6	0.4
10 min SE <i>Populus</i>	0.2	6.0	61.4	0.2	1.5	30.1	0.5

**Table 2**  
The maximum amount of direct orange and blue dye adsorbed by untreated and pretreated *Populus* expressed as mg dye/g substrate during Simons' stain.

Substrate ( <i>Populus</i> )	Maximum adsorbed orange dye (mg/g sample)	Maximum adsorbed blue dye (mg/g sample)	Total adsorbed dye (mg/g sample)	O/B ratio
Untreated	10.6	56.4	67.0	0.19
10 min SE	16.1	64.6	80.7	0.25
10 min DAP	28.3	71.8	100.1	0.39
60 min DAP	44.8	83.3	128.1	0.54

### 3.2. Simons' stain

Simons' stain method evaluates the accessibility of a substrate by applying two different dyes: direct orange and direct blue. Dyes are well known as sensitive probes for the characterization of cellulose structure, and direct dyes are particularly appropriate because of their linear structures and outstanding substantivity toward cellulose (Inglesby and Zeronian, 2002). Direct blue 1 has a well-defined chemical formula with a molecular weight of 992.82 g/mol and a molecular diameter of  $\sim 1$  nm. Direct orange 15 is a condensation product of 5-nitro-*o*-toluenesulfonic acid in aqueous alkali solution, with a molecular diameter in the range of  $\sim 5$ –36 nm. When lignocellulosic biomass is treated with a mixed solution of the direct orange and blue dye, the blue dye enters all the pores with a diameter larger than  $\sim 1$  nm, while the orange dye only populates the larger pores. After a pore size increase either by physical or chemical action, the orange dye will gain further access to the enlarged pores because of the higher affinity of the orange dye for the hydroxyl groups on a cellulosic surface. The ratio and amount of direct orange (DO) and direct blue (DB) dye adsorbed into the biomass can be used to indicate the amount of large pores to small pores and subsequently cellulose accessibility in lignocellulosic biomass for enzymatic deconstruction (Chandra et al., 2008). The maximum amount of dye adsorbed to the lignocellulosic substrates was calculated using the Langmuir adsorption equation:

$$[C]/[A] = 1/(K_{ads}[A]_{max}) + [C]/[A]_{max} \quad (1)$$

where  $[C]$  (mg/mL) is the free dye concentration,  $[A]$  (mg/mg) is the amount of dye adsorbed by the substrate,  $K_{ads}$  is Langmuir adsorption constant, and  $[A]_{max}$  is the maximum amount of dye adsorbed. The Langmuir isotherm plot, which is prepared by plotting  $[C]/[A]$  versus  $[C]$ , yields a slope =  $1/[A]_{max}$ . The maximum amount of dye adsorbed by the substrate can be then obtained from the Langmuir isotherm curves.

The ratio of adsorbed DO and DB (i.e., O/B ratio) is a common value used to estimate the relative porosity and assess the overall accessible surface area of cellulose to cellulases. Chandra et al. (2008) found that the use of SS dyes, more specifically the O/B ratio, as a molecular probe is a good indicator of the total surface area of cellulose available to the enzymes. It was also evident that the higher the O/B ratio, the lower the protein loading required for efficient hydrolysis (Arantes and Saddler, 2011). As mentioned above, the adsorbed O/B ratio has been related to cellulose accessibility and cellulase activity; however, it can be helpful to also

analyze the total amount of dye adsorbed. For example, as SSA become significant and large proportions of pores are small in size, large amounts of the smaller DB dye are adsorbed by a substrate and cause a decrease in the overall O/B ratio. In this case, there may be a significant amount of large pore and cellulose accessibility, but analysis based solely on the low O/B ratio may skew data interpretation. An increase in the adsorbed O/B ratio accompanied by a minimal increase in total dye adsorption generally indicates a larger accessible surface area. A comparison of the O/B ratio before and after treatment is indicative of an expansion of existing pores. Again, when comparing SS results before and after treatment, a minimal increase in the adsorbed O/B ratio with large increases in total dye adsorption suggests pore generation is occurring.

As shown in Table 2, *Populus* showed an increase of the total amount of adsorbed dye after pretreatment, for all conditions, when compared to the untreated sample. Table 2 also indicates that total dye adsorption increases with pretreatment severity with the smallest increase shown for the 10 min SE sample, then 10 min DAP, and finally with the largest increase for the 60 min DAP sample. Both the adsorption of DO and DB dye increased after pretreatment, but the adsorption of the orange dye increased to a higher extent than the adsorption of the blue dye after pretreatment. This asymmetrical increase caused the O/B ratio to increase with pretreatment severity, increasing from 0.19 (untreated sample) to 0.25 (10 min SE sample), 0.39 (10 min DAP sample), and 0.54 (60 min DAP sample), respectively. These results suggest that both DAP and SE increase SSA by generating new pores and expanding the size of existing pores, and DAP increases SSA as a function of pretreatment severity. The results also indicate, despite explosive decompression that occurs during SE, under a similar time and temperature profile DAP is more effective in terms of the overall accessible surface area incensement.

As shown previously, both DAP and SE are ineffective at the removal of the majority of lignin, and the acid insoluble lignin content actually increases after DAP. The SS results showed that, in spite of higher lignin content, pretreatment especially DAP results in a much larger accessible cellulosic surface area. Hsu et al. (2010) suggested that this was not only caused by hemicellulose removal but also by hydrolysis and rearrangement of the lignin structure during DAP. Wiman et al. (2012) also found that although the lignin content of the steam-pretreated spruce increased at higher pretreatment temperature and residence time, the initial rate of enzymatic hydrolysis increased, and the DR 28 (Congo Red) stain and Simons' stain indicated that pretreatment did not result in larger total cellulosic surface areas but rather in a larger accessible

cellulosic surface area. So the positive effects of cellulose accessibility thus dominate over the negative effects of lignin for steam-pretreated spruce. However, highly selective lignin removal is also important to pinpoint the lignin effect on biomass digestibility but has rarely been reported for application of delignification to pretreated biomass, and the chemical reagents employed to delignify pretreated biomass are known oxidizing agents (sodium chlorite-acetic acid and peracetic acid) and, therefore, can affect cellulose structure features such as crystallinity, degree of polymerization, and subsequently accessibility (Kumar et al., 2013).

### 3.3. NMR cryoporometry

NMR cryoporometry is a technique for non-destructively determining pore size distribution (PSD) in porous media through the observation of the depressed melting point of a confined liquid. It takes advantage of the fact that small crystals formed from liquid within pores melt at a lower temperatures than bulk liquid, which is known as melting point depression caused by enthalpic interaction with the pore surface. For a liquid confined within a pore in which a crystal is forming, the melting point depression of the liquid can be related to pore surface area to volume ratio or more specifically pore size through the Gibbs–Thompson equation (Strange et al., 1993):

$$\Delta T = T_m - T_m(x) = k/x \quad (2)$$

where  $T_m$  is the normal melting point,  $T_m(x)$  is the melting point of a crystal in pores of diameter  $x$ , and  $k$  is a characteristic constant of the liquid. The pore fluid volume  $v$  is a function of pore diameter  $x$ , so the melting temperature of the liquid  $T_m(x)$  can be related to the pore size distribution by:

$$\frac{dv}{dx} = \frac{dv}{dT_m(x)} \frac{dT_m(x)}{dx} \quad (3)$$

From Eq. (2),  $dT_m(x)/dx = k/x^2$ , so Eq. (3) becomes

$$\frac{dv}{dx} = \frac{dv}{dT_m(x)} \frac{k}{x^2} \quad (4)$$

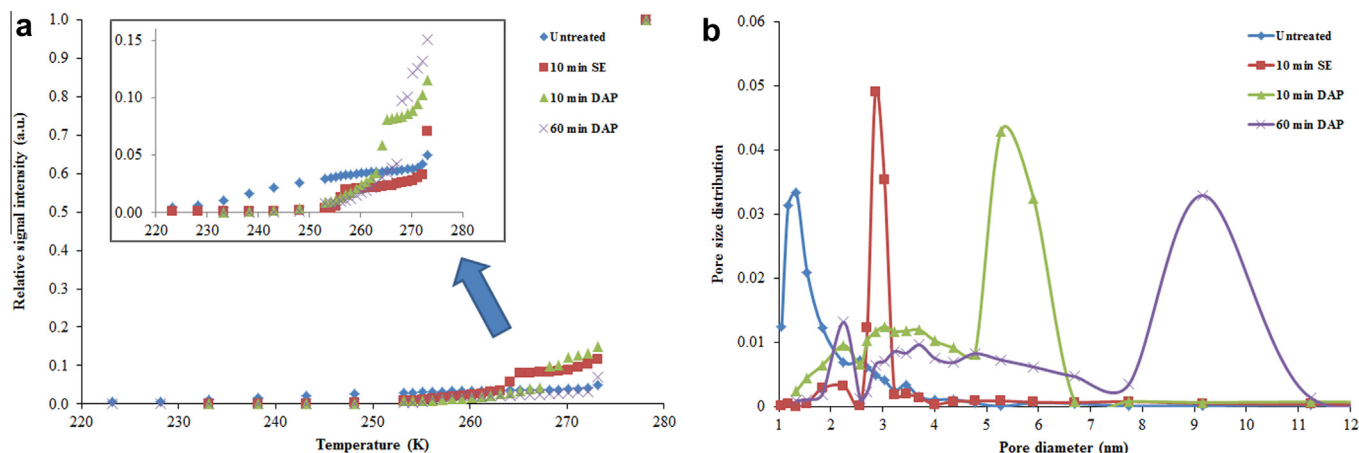
The NMR cryoporometry data contains a signal intensity proportional to the integral pore fluid volume  $v$ , which varies as a function of temperature  $T$ . At each temperature,  $v$  is the volume of liquid in cell wall pores with a dimension less than or equal to  $x$  as given by Eq. (3). So the measurement of  $dv/dT_m(x)$  which can be obtained from the slope of the curve of  $v$  against  $T$ , provided  $k$  is known for the liquid used (50.0 K·nm for water) will allow the pore size distribution curve to be determined.

Fig. 1(a) shows the melting curves (e.g., the temperature dependences of the NMR signal intensity) of all the samples in the range

of temperatures between 220 and 280 K. The intensities measured at each temperature  $T$  were corrected according to Curie's law by multiplication with the factor  $T/T_0$  to account for the temperature dependence of the occupation of the spin levels under the assumption of a linearized Boltzmann distribution. The corrected intensities are normalized to the value just below  $T_0 = 280$  K, where all pore water as well as excess water are in the liquid state. A step-like intensity increase in the vicinity of the bulk melting point of water 273 K was observed for all the samples, which is attributed to the bulk liquid component. The smooth increase of the signal intensity with temperature in the region of pore melting indicates a transition of water in the pores. According to the Gibbs–Thompson equation, liquid melting depression is inversely proportional to the pore diameter; therefore, liquid in smaller pores has a lower melting point which means as temperature increases, liquid in smaller pores starts melting first. As shown in Fig. 1(a), as the temperature increases, the NMR intensity for untreated sample starts to increase first, and this change refers to the melting of water in small pores of the untreated material. The pore size distribution of these lignocellulosic biomass samples calculated based on Gibbs–Thompson equation using the first derivative of the intensity with respect to temperature ( $dv/dT_m(x)$ ) from the melting curve is shown in Fig. 1(b). A representative pore diameter can be roughly estimated from peak maximums. The positions of the main peaks attributed to micro-/meso-scale pores in the PSD for untreated, 10 min SE, 10 min DAP, and 60 min DAP sample are 1.5 nm, 3 nm, 6 nm, and 9 nm, respectively. Only DAP samples seem to have the nominal size required for cellulase (diameter  $\sim 5.1$  nm) access. Obviously, all the pretreated samples display a larger pore diameter than the untreated sample. In addition, the two 10 min pretreatments (of both SE and DAP) have a broad pore diameter polydispersity with a broader distribution of pore diameters observed for DAP than for SE. However, due to the lack of experimental points at temperature near 0 °C this broadening effect could be a result of noise. The pore size shows up in bimodal distribution after pretreatment in the mesoporous range. All the pretreatments cause the formation of an additional peak, centered around 2.2 nm, which again indicates that pretreatment most likely causes pore expansion.

### 3.4. NMR relaxometry

Like NMR cryoporometry, there are other NMR based techniques which can be used to track changes in accessibility upon treatment of biomass, such as proton NMR relaxometry. Adsorbed water can be found spatially localized within intra-lamellar



**Fig. 1.** (a) Melting curves (temperature dependence of NMR signal intensity) of untreated and pretreated *Populus* samples. (b) Pore size distributions of untreated and pretreated *Populus* samples calculated using the Gibbs–Thompson equation.

microreticular pores situated at microfibril surfaces, within the lignin-hemicellulose matrix, existing as capillary water in the lumen, or between fibers as surface water (Menon et al., 1987). The nature and strength of the association between the probe molecule, water, and the cell wall is directly related to the ultrastructural and chemical state of the biomass (Felby et al., 2008). Therefore by monitoring the amount and the relative nature of nuclear relaxation seen in the adsorbed water, information about changes in biomass pore surface area to volume ratio and chemistry can be inferred.

In this work,  $^1\text{H}$   $T_2$  data measured with the CPMG sequence and analyzed via inverse Laplace transformation (ILT) were used to investigate the change in the nature of biomass–water interactions and subsequent accessibility as a result of DAP and SE. Biomass, for example, with a more hydrophilic pore surface chemistry and/or reduced pore size distributions will contain a higher proportion of bound to unbound water. This would be reflected in NMR cryoporometry by greater melting point temperature depression. NMR relaxation experiments can provide information pertaining to the molecular mobility within a system. In a spin–spin or  $T_2$  relaxation curve, the signal intensity decays as a function of local inhomogeneities in the magnetic field mainly due to perturbation by nuclei through dipolar interactions (Araujo et al., 1993). This attenuation is described by a characteristic relaxation time referred to as the  $T_2$  relaxation time. Basically, as the  $T_2$  relaxation time of adsorbed water increases, the degrees of freedom or average local mobility of the water in the pores also increases. Similarly, an increase in  $T_2$  relaxation time of adsorbed water can be correlated with a decrease in the proportion of bound to unbound water or amount of water located at pore surface versus the pore interior. Therefore, in systems of increasing average pore size, the pore surface area to volume ratio will decrease and is therefore detected by an increase in the  $T_2$  relaxation time. As determined by a CPMG experiment the  $T_2$  time of free water is  $\sim 3$  s.

A common technique to extract information for comparison on systems having wide distributions of nuclear relaxers or  $T_2$  decays utilizes an inverse Laplace transforms (ILT) routine (Felby et al., 2008). Supplementary Fig. S1(a) depicts the relaxation time distributions of adsorbed water in untreated and pretreated *Populus* wood as a result of ILT. The  $T_2$  distribution of adsorbed water in the untreated wood chip sample shows the existence of at least two pools of adsorbed water with  $T_2$  peaks centered at 11.5 and 40.5 ms. The exact location in the cell wall of these pools of water is difficult to determine; however, based on studies investigating relaxation rates of plant cell wall physiological water distributions in wood during drying (Menon et al., 1987), water within the meso-scale pores of the lignin-hemicellulose matrix and in wood lumen/capillary structures represent the downfield and upfield peaks. Despite the exact location of the water distributions, Supplementary Fig. S1(a) indicates significant expansion of the larger cell wall water pool seen in the untreated sample centered at  $\sim 40.5$  ms with pretreatment. Interestingly, increasing DAP time from 10 to 60 min only causes a slight increase in  $T_2$  times, whereas upon SE, even for a short residence time, a much larger increase is observed. This would suggest the mechanism related to a decrease in the pore surface area to volume ratio and an increase in accessibility as a result of DAP pretreatment occurs primarily in the first 10 min of pretreatment, and though continues through the remaining 50 min of pretreatment, happens at a significantly slower rate. The results also show that SE is much more effective at decreasing the pore surface area to volume ratios, at least for the cell wall water pools detected by changes in  $T_2$  relaxation times.

It is also well known that liquid molecules near a solid surface will have different spin–lattice or  $T_1$  relaxation profiles from that of the bulk liquid because of interactions at the solid–liquid interface (Haggkvist et al., 1998; Li et al., 1993). As a result, in porous biomass that contains water the observed average  $T_1$  time of the

adsorbed water is influenced by the surface area to volume ratio of the pores. Under fast exchange conditions, there are models describing the change in  $T_1$  relaxation, based on a two-component system, where the observed  $T_1$  is the weighted sum of relaxation times of free and surface bound water. However,  $T_1$  relaxation is more sensitive to higher frequency relaxation and molecular dynamics than  $T_2$  relaxation, the consequence being a lowered ability to detect (1) pore surface bound water and (2) differences in pore sizes, especially for larger pore systems. Nevertheless, analyzing  $T_1$  relaxation of adsorbed cell wall water can be informative particularly in light of the well-developed model describing changes in  $T_1$  relaxation due to fast exchange between pore surface bound and unbound water. Much like the  $T_2$  analysis above,  $^1\text{H}$  inversion recovery experiments and ILT of  $T_1$  relaxation curves were generated and used to investigate the changes in accessibility as a result of pretreatment.

ILT of the  $T_1$  relaxation curve of the untreated *Populus* biomass shows the existence at least one pool of cell water adsorbed into biomass with  $T_1$  times centered at  $\sim 0.60$  s. All pretreatments cause the development of the second upfield distribution and a slight increase in the  $T_1$  times of the peak seen in the untreated sample. As in  $T_2$  relaxation, increases in  $T_1$  time suggest that more free water exist within the biomass, with free water having a  $T_1$  time of  $\sim 2.2$  s. Fig. S1(b) seems to indicate a similar significant decrease in the pore surface area to volume ratio occurs in the cell wall of *Populus* biomass upon pretreatment. The relative intensities of the two water distributions suggest the SE sample has more water in the larger dimension cell wall water pool than in the DAP samples.

### 3.5. NMR diffusometry and $q$ -space imaging

Another property of the solvent probe molecule that can be gathered in a fairly straightforward manner by NMR measurement is the self-diffusion coefficient. An increase in pore size distributions can be reflected by the increase of diffusion coefficient due to increased unrestricted diffusion path lengths and decreased fractions of pore surface bound water. Pulsed gradient spin echo (PGSE) experiments have been in wide use to investigate molecular diffusion of fluids in various porous systems (e.g., biomass) (Tanner and Stejskal, 1968). Typically, this method is used to determine the apparent self-diffusion coefficient ( $D_s$ ) of a molecule. This can be done using the following equation:

$$\frac{I}{I_0} = \exp \left[ (-\gamma G \delta)^2 D_s \left( \Delta - \frac{\delta}{3} \right) \right] = \exp \left[ -(2\pi q)^2 D_s \left( \Delta - \frac{\delta}{3} \right) \right] \quad (5)$$

where  $\gamma$  is the nuclear gyromagnetic ratio,  $G$  is the gradient strength,  $\delta$  is the amount of time the gradient is applied ( $q = G\delta\gamma/2\pi$ ) and  $\Delta$  is delay between the application of the gradients (Topgaard and Soederman, 2001). By systematically varying either  $G$ ,  $\delta$ , or  $\Delta$  the  $D_s$  of a system can be determined. Also, by using a well-defined  $(\Delta - \delta/3)$  interval or period of observation PGSE experiments can probe the diffusion of a molecule over various length scales. The larger the interval, the longer the technique “observes” or the larger the root-mean distance of observation in which the diffusion coefficient is determined over (Foston and Ragauskas, 2010; Li et al., 1997).

As done above,  $^1\text{H}$  PGSE experiments and ILT of diffusion attenuation curves were generated and used to investigate the changes in accessibility as a result of pretreatment. The resulting distribution of  $D_s$ , detected with an observation window of  $\Delta = 100$  ms, for water adsorbed in untreated and pretreated *Populus* biomass is shown in Fig. S1(c). In general, an increase in pore size distributions could cause the average  $D_s$  to increase due to a lower fraction of pore surface bound water or larger unobstructed root-mean

diffusion path ( $D_s$  of bulk free water is  $\sim 2.27 \times 10^{-9} \text{ m}^2 \text{ s}^{-1}$ ). The  $D_s$  distributions, seen in Fig. S1(c), indicate there is at least one resolvable  $D_s$  within the untreated *Populus* biomass centered at  $\sim 1.06 \times 10^{-10} \text{ m}^2 \text{ s}^{-1}$ . All pretreatments cause the development of additional fast diffusion coefficients and a slight increase in the  $D_s$  of the peak seen in the untreated sample. SE pretreatment specifically causes the development of two new distributions, which seems to suggest the explosive decompression results in a more complex pore system.

An alternative method of analyzing PGSE techniques utilizes q-space NMR imaging to characterize the average pathway of liquid molecules imbibed in a micro-porous medium, the plant cell wall (Li et al., 1997). Water displacement probability profiles can be obtained by Fourier transform of the spin-echo attenuation profiles measured as a function of the changing gradient amplitude or  $q$ . The displacement probability profiles describe the probability that water undergoing random diffusive motion will encounter a wall. These water displacement probability profiles were collected on untreated and pretreated *Populus* biomass for varying diffusion observation times ( $\Delta = 25\text{--}200 \text{ ms}$ ). Several studies have demonstrated that water translational displacement probability profiles can be obtained directly by Fourier transform of the spin-echo attenuation profiles ( $E[q]$ ) recorded as a function of the magnitude of the pulsed field gradient at a fixed gradient spacing for both cellulose fiber and wood pulps (Stilbs, 1987).

$$E(q) = \int \int \rho(r)Ps(r|r', \Delta) \exp[i2\pi q(r' - r)]dr' dr \quad (6)$$

where  $r' - r$  represents the displacement distance. This type of q-space imaging experiments can provide a novel method to produce data of microscopic spacing in porous media, at a higher spatial resolution than  $k$ -space images generated from more traditional NMR imaging. Fig. 2 shows characteristic diffusion NMR data sets plotted as the echo intensity versus the magnitude of the wave number vector  $q$  (spin-echo attenuation profiles). This was done for four different diffusion observations or  $\Delta$ -values 25, 50, 100 and 200 ms (only  $\Delta = 100 \text{ ms}$  curves are shown in Fig. 2. One data processing option is to determine apparent diffusion coefficient using Eq. (6). In this case the result from the diffusion attenuation curves can be affected by cross-relaxation with the biomass, anisotropic diffusion, and pore tortuosity.

However, in an effort to extract a distribution which can represent the pore sizes on a macro-scale, the spin-echo attenuation profiles were converted to a complex form, zero filled to 256 points, and inverted using a Fourier transform algorithm using Matlab software. The resulting distribution is a water displacement probability profile, which describes the probability water undergoing random diffusive motion will encounter a pore wall. Based on the Fig. 3, an average diffusion displacement plot at an observation window of  $\Delta = 100 \text{ ms}$ , it is clear that the untreated *Populus* biomass has a much higher relative intensity centered at shorter displacement probability values than pretreated samples, with the lowest relative intensity for the SE sample. This clearly shows a difference in micron related pores as a result of difference pretreatment. Again there is little difference between 10 min and 60 min DAP sample, suggesting the majority of increases in accessibility

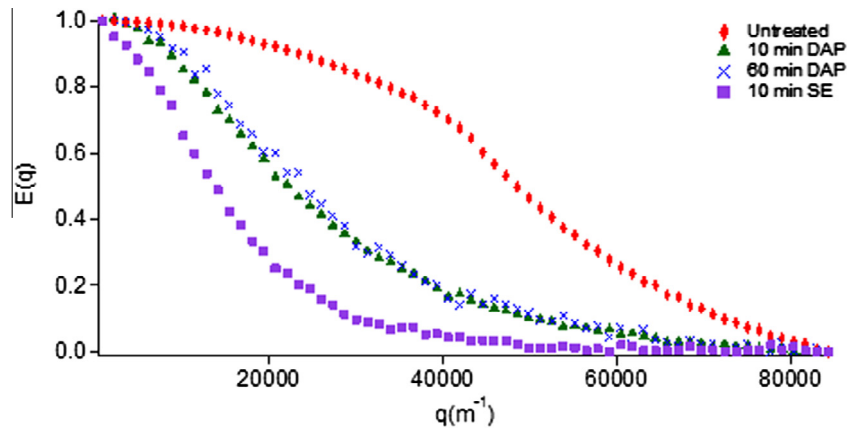


Fig. 2. Echo amplitude as a function of  $q = G\delta\gamma/2\pi$  at  $\Delta = 100 \text{ ms}$  of water in untreated and pretreated *Populus* biomass at a moisture content of  $60 \pm 3\%$ .

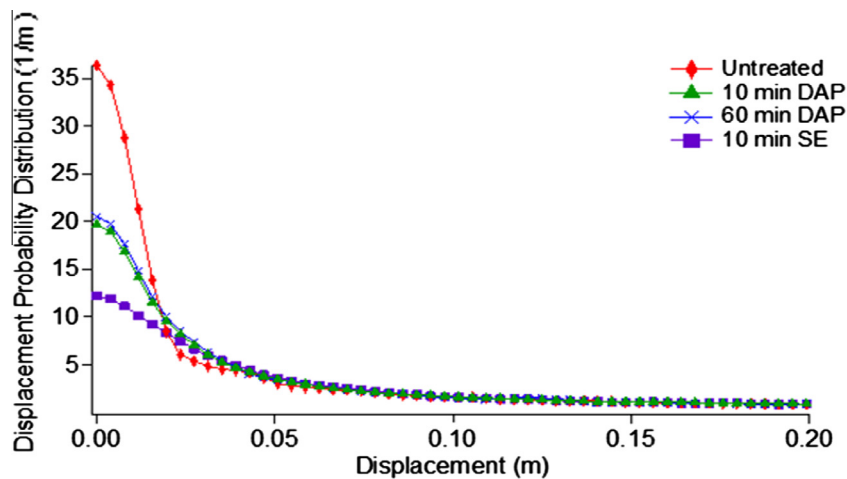


Fig. 3. Average diffusion displacement of water in untreated and pretreated *Populus* biomass at a moisture content of  $60 \pm 3\%$  ( $\Delta = 100 \text{ ms}$ ).

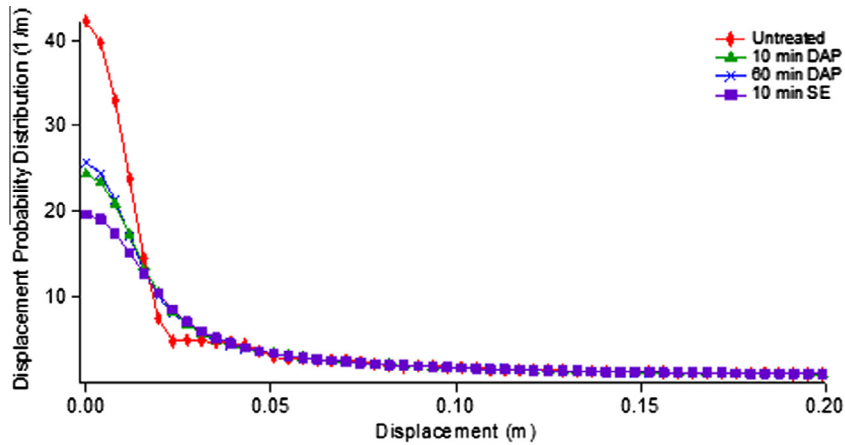


Fig. 4. Average diffusion displacement of water in untreated and pretreated *Populus* biomass at a moisture content of  $60 \pm 3\%$  ( $\Delta = 25$  ms).

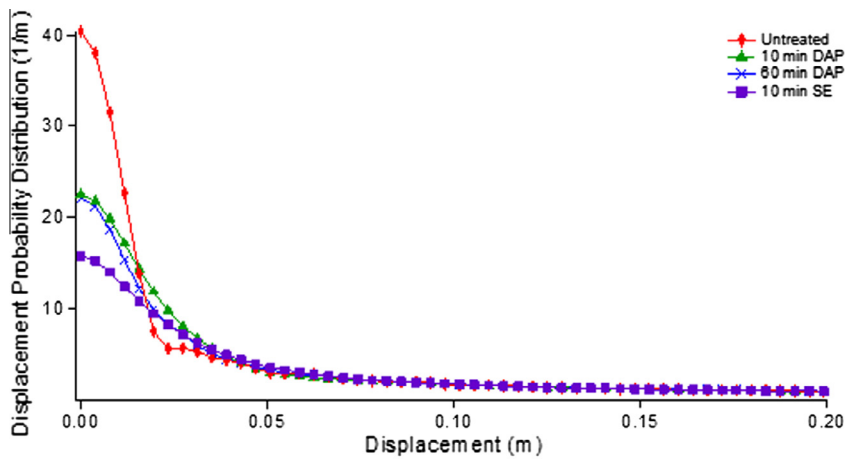


Fig. 5. Average diffusion displacement of water in untreated and pretreated *Populus* biomass at a moisture content of  $60 \pm 3\%$  ( $\Delta = 50$  ms).

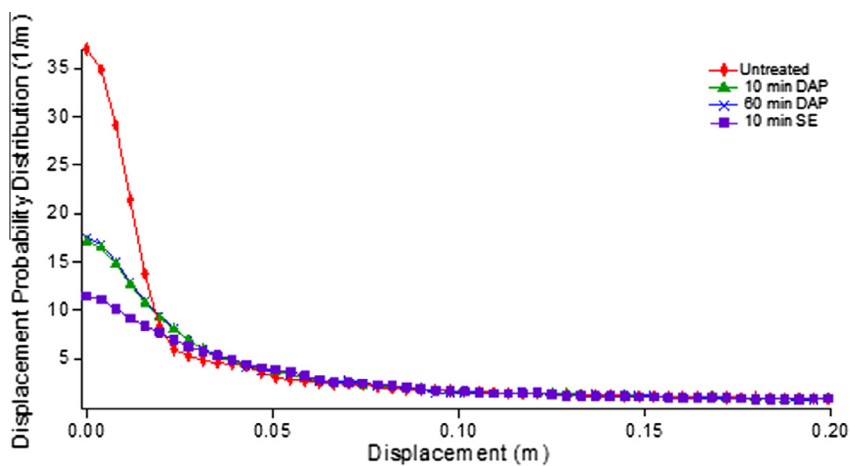


Fig. 6. Average diffusion displacement of water in untreated and pretreated *Populus* biomass at a moisture content of  $60 \pm 3\%$  ( $\Delta = 200$  ms).

occurs in the first 10 min of DAP and that the cell wall expansion in SE pretreatment, at least in cell wall water pools, is more effective. Other average diffusion displacement plots at observation windows of  $\Delta = 25, 50,$  and  $200$  ms are shown in Figs. 4–6, and display similar results as Fig. 3.

Eq. (6) suggests these displacement probability profiles should be Gaussian and have been shown to follow the form:

$$P(R, \Delta) = A * \exp\left(-\frac{(r' - r)^2}{Ds}\right) \quad (7)$$

**Table 3**

The apparent self-diffusion ( $D_s$ ) coefficient of water as a result of the perturbing effect of pore in the plant cell wall of *Populus* in  $\text{m}^2/\text{s}$ .

Substrate	$\Delta = 25$ ms	$\Delta = 50$ ms	$\Delta = 100$ ms	$\Delta = 200$ ms
Untreated	$1.9 \times 10^{-6}$	$9.1 \times 10^{-7}$	$6.6 \times 10^{-7}$	$3.2 \times 10^{-7}$
10 min DAP	$6.7 \times 10^{-6}$	$4.0 \times 10^{-6}$	$3.0 \times 10^{-6}$	$2.0 \times 10^{-6}$
60 min DAP	$6.2 \times 10^{-6}$	$4.5 \times 10^{-6}$	$2.7 \times 10^{-6}$	$2.0 \times 10^{-6}$
10 min SE	$1.1 \times 10^{-5}$	$9.4 \times 10^{-6}$	$8.2 \times 10^{-6}$	$5.2 \times 10^{-6}$

Where  $A = \frac{1}{2\sqrt{\pi\Delta D_s}}$  and  $D_s$  is the measure diffusion coefficient for water in the plant cell wall accounting for the perturbing effect of the porous system. Fig. S2 shows the Gaussian fit to the water displacement probability profile on 10 min steam explosion pretreated wood sample at a diffusion time of 100 ms. This analysis was done on all samples for all diffusion times and tabulated in Table 3. In general, the trends show the  $D_s$  slows with increase diffusion time and increases from the untreated sample to the pretreated samples. This again suggests that pretreatment significantly increases the size of pores with respect to untreated samples.

When the measurement of pore size or accessible surface area in the lignocellulosic cell wall is discussed, it is important to realize that different techniques can give considerably different results, due to the differences in the principles of measurement between the techniques. For example, the mean pore diameter of pine kraft fibers was determined by solute exclusion technique to be around 3 nm; however, it is significantly higher when measured by an NMR technique, about 13 nm (Suurnakki et al., 1997). Table 4

summarizes the SSA and porosity reported in literature using different techniques as well as its advantages and disadvantages.

In terms of the techniques used in this study, for DAP, the PSD generated by cryoporometry show that the 10 min and 60 min pretreated *Populus* have mean diameters around 6 and 9 nm, both should have enough large pores accessible to the orange dye used in SS. However, SS results show that the increase of pretreatment time from 10 min to 60 min causing orange dye adsorption increases from 28.3 to 44.8 mg/g. Cell wall expansion could obviously increase the cellulose accessible surface area. However, considering the fact that both 10 min and 60 min DAP sample have enough large pores accessible to the orange dye, this increased dye adsorption may be due to the extensive removal of hemicellulose caused by increased pretreatment time. In other words, the significant increase of orange dye adsorption may not be due to a result of significant pore expansion, in fact, the NMR relaxometry and diffusometry revealed that pore expansion for DAP occur primarily in the first 10 min. The cryoporometry only indicates pores up to 10 nm in this study; there are clearly larger pores than that which SS,  $T_1$ ,  $T_2$  and diffusion test all can detect. However, the SS test is sensitive to pore inlet size. If a pore is large but the entrance to that pore is small, the SS methodology will not reflect the existence of that large pore. Relaxometry and diffusometry, not affected by pore inlet size, indicate that SE is more effective at pore expansion, while SS results show that orange dye adsorption for 10 min SE is only 16.1 mg/g. As mentioned before, the voids left by hydrolyzed hemicellulose are important, and another explanation could be the possible generation of some “ink-bottle” shaped pores

**Table 4**

Characterization of cellulose accessibility before and after pretreatment by different techniques (Keshwani and Cheng, 2010; Arantes and Saddler, 2011; Thompson et al., 1991; Grethlein, 1985; Wiman et al., 2012; Foston and Ragauskas, 2010; Ostlund et al., 2010).

Biomass substrates	Analytical techniques	Cellulose accessibility		Advantages and disadvantages
Untreated switchgrass	Simons' stain	Orange/blue ratio	0.08	Advantages:
Calcium hydroxide pretreated switchgrass			0.26	◆ Measurement can be done in wet state
Sodium hydroxide pretreated switchgrass			0.39	◆ Relatively fast, simple and accurate
Steam pretreated lodgepole pine			0.65	◆ Ability to measure interior and exterior surface area
Steam pretreated douglas fir			0.85	Disadvantages:
Ethanol organosolvpretreated poplar			1.20	◆ Effected by pore shape and tortuosity
Untreated mixed hardwood	Solute exclusion	Specific surface area available to solute of 5.1 nm diameter ( $\text{m}^2/\text{g}$ )	14.8	◆ Not fully quantitative
Hydrogen peroxide pretreated mixed hardwood			24.5	Advantages:
Ethylendiamine pretreated mixed hardwood			30.7	◆ Quantitatively measurement of pore volume in wet state
Untreated poplar		Pore volume accessible to solute of 5.1 nm diameter (ml/g)	0.03	Disadvantages:
Sulfuric acid pretreated poplar			0.45	◆ Laborious, unspecific to cellulose, does not account for the external surface area
Untreated white pine			0.10	◆ Irregular shapes, such as “ink-bottle” effect the accuracy
Sulfuric acid pretreated white pine			0.38	
Untreated spruce	Nitrogen adsorption	Brunauer-Emmett-Teller (BET) surface area ( $\text{m}^2/\text{g}$ )	0.4	Advantages:
2% $\text{SO}_2$ pretreated spruce at 194 °C			1.3	◆ Accurate, robust method for determining the surface are accessible nitrogen molecule
2% $\text{SO}_2$ pretreated spruce at 220 °C			8.2	Disadvantages:
1% $\text{SO}_2$ pretreated spruce at 207 °C			2.7	◆ Measurement requires dry sample
2.9% $\text{SO}_2$ pretreated spruce at 207 °C			6.3	◆ Small size of nitrogen cause over-estimation of cellulose accessibility
Never dried pulp	NMR	Cumulated pore volume from 2 to 10 nm ( $\text{cm}^3/\text{g}$ )	0.064	Advantages:
Bench dried pulp	Cryoporometry		0.062	◆ Not affected by pore inlet size or shape
Oven dried pulp			0.044	◆ Non-destructive measurement
Untreated poplar	NMR relaxometry	Average spin-lattice $T_1$ times of $\text{D}_2\text{O}$ within biomass (ms)	23.9	Disadvantages:
5 min DAP poplar			27.8	◆ Expensive, requires complicated setup and long experiment time
10 min DAP poplar			32.0	
60 min DAP poplar			36.3	

caused by explosive decompression during SE prevents orange dye access. However, that large pore is more than likely inaccessible to cellulolytic enzymes as well. In addition, DAP has also been shown to increase the pore tortuosity within the biomass (Foston and Ragauskas, 2010), which also affects the SS test results significantly. Lastly, the effect of lignin rich pore surfaces on dye adsorption during this modified SS testing is fairly unclear.

#### 4. Conclusion

A modified SS technique, in combination with NMR analysis, revealed that DAP and SE increases the pore size distribution and SSA of a lignocellulosic substrate such that appreciable amounts of enzymes could have access to cellulose. The results show DAP is more effective than SE in terms of increasing SSA, and that as DAP severity is increased, so is SSA. NMR relaxometry and diffusometry indicate that pore expansion for DAP pretreatment occurs primarily in first 10 min of pretreatment, but SE is more effective at pore expansion for the cell wall water pools detected by changes in relaxation times.

#### Acknowledgements

This manuscript has been authored by Georgia Tech under Subcontract No. 4000116095 and Contract No. DE-AC05-00OR22725 with the U.S. Department of Energy. The United States Government retains and the publisher, by accepting the article for publication, acknowledges that the United States Government retains a non-exclusive, paid-up, irrevocable, world-wide license to publish or reproduce the published form of the manuscript or allow others to do so, for United States Government purposes.

#### Appendix A. Supplementary data

Supplementary data associated with this article can be found, in the online version, at <http://dx.doi.org/10.1016/j.biortech.2013.06.091>.

#### References

- Arantes, V., Saddler, J.N., 2011. Cellulose accessibility limits the effectiveness of minimum cellulase loading on the efficient hydrolysis of pretreated lignocellulosic substrates. *Biotechnol. Biofuels* 4, 3.
- Araujo, C.D., Mackay, A.L., Whittall, K.P., Hailey, J.R.T., 1993. A Diffusion model for spin–spin relaxation of compartmentalized water in wood. *J. Magn. Reson. Ser. B* 101, 248–261.
- Chandra, R., Ewanick, S., Hsieh, C., Saddler, J.N., 2008. The characterization of pretreated lignocellulosic substrates prior to enzymatic hydrolysis, part 1: a modified Simons' staining technique. *Biotechnol. Prog.* 24, 1178–1185.
- Chen, Y., Wang, Y., Wan, J., Ma, Y., 2010. Crystal and pore structure of wheat straw cellulose fiber during recycling. *Cellulose* 17, 329–338 (Dordrecht, Neth.).
- Choudhary, R., Umagiliyage, A.L., Liang, Y., Siddaramu, T., Haddock, J., Markevicius, G., 2012. Microwave pretreatment for enzymatic saccharification of sweet sorghum bagasse. *Biomass Bioenergy* 39, 218–226.
- Esteghlalian, A.R., Bilodeau, M., Mansfield, S.D., Saddler, J.N., 2001. Do enzymic hydrolyzability and Simons' stain reflect the changes in the accessibility of lignocellulosic substrates to cellulase enzymes? *Biotechnol. Prog.* 17, 1049–1054.
- Felby, C., Thygesen, L.G., Kristensen, J.B., Jorgensen, H., Elder, T., 2008. Cellulose-water interactions during enzymatic hydrolysis as studied by time domain NMR. *Cellulose (Dordrecht, Neth.)* 15, 703–710.
- Foston, M., Ragauskas, A.J., 2010. Changes in the structure of the cellulose fiber wall during dilute acid pretreatment in *Populus* studied by  $^1\text{H}$  and  $^2\text{H}$  NMR. *Energy Fuels* 24, 5677–5685.
- Grethlein, H.E., 1985. The effect of pore size distribution on the rate of enzymatic hydrolysis of cellulosic substrates. *Biotechnology* 3 (2), 155–160.
- Haggkvist, M., Li, T.-Q., Odberg, L., 1998. Effects of drying and pressing on the pore structure in the cellulose fiber wall studied by proton and deuteron NMR relaxation. *Cellulose (London)* 5, 33–49.
- Hsu, T.-C., Guo, G.-L., Chen, W.-H., Hwang, W.-S., 2010. Effect of dilute acid pretreatment of rice straw on structural properties and enzymatic hydrolysis. *Bioresour. Technol.* 101 (13), 4907–4913.
- Hu, F., Jung, S., Ragauskas, A.J., 2012. Pseudo-lignin formation and its impact on enzymatic hydrolysis. *Bioresour. Technol.* 117, 7–12.
- Keshwani, D.R., Cheng, J.J., 2010. Microwave-based alkali pretreatment of switchgrass and coastal bermudagrass for bioethanol production. *Biotechnol. Prog.* 26 (3), 644–652.
- Kumar, R., Hu, F., Hubbell, C.A., Ragauskas, A.J., Wyman, C.E., 2013. Comparison of laboratory delignification methods, their selectivity, and impacts on physicochemical characteristics of cellulosic biomass. *Bioresour. Technol.* 130, 372–381.
- Inglesby, M.K., Zeronian, S.H., 2002. Direct dyes as molecular sensors to characterize cellulose substrates. *Cellulose (Dordrecht, Neth.)* 9, 19–29.
- Li, T.Q., Haeggkvist, M., Odberg, L., 1997. Porous structure of cellulose fibers studied by Q-space NMR imaging. *Langmuir* 13, 3570–3574.
- Li, T.Q., Henriksson, U., Odberg, L., 1993. Determination of pore sizes in wood cellulose fibers by deuterium and proton NMR. *Nord. Pulp Pap. Res. J.* 8, 326–330.
- Mansfield, S.D., Mooney, C., Saddler, J.N., 1999. Substrate and enzyme characteristics that limit cellulose hydrolysis. *Biotechnol. Prog.* 15, 804–816.
- Menon, R.S., MacKay, A.L., Hailey, J.R.T., Bloom, M., Burgess, A.E., Swanson, J.S., 1987. An NMR determination of the physiological water distribution in wood during drying. *J. Appl. Polym. Sci.* 33, 1141–1155.
- Ostlund, A., Kohnke, T., Nordstierna, L., Nyden, M., 2010. NMR cryoporometry to study the fiber wall structure and the effect of drying. *Cellulose (Dordrecht, Neth.)* 17 (2), 321–328.
- Pu, Y., Zhang, D., Singh, P.M., Ragauskas, A.J., 2008. The new forestry biofuels sector. *Biofuels Bioprod. Biorefin.* 2, 58–73.
- Ragauskas, A.J., Williams, C.K., Davison, B.H., Britovsek, G., Cairney, J., Eckert, C.A., Frederick Jr., W.J., Hallett, J.P., Leak, D.J., Liotta, C.L., Mielenz, J.R., Murphy, R., Templer, R., Tschaplinski, T., 2006. The path forward for biofuels and biomaterials. *Science (Washington, DC, US)* 311, 484–489.
- Simitzis, A., Sfyrakis, J., Faliagas, A., 1995. Characterization of pore structure by porosimetry and sorption on adsorbent produced from novolac-biomass. *Mater. Chem. Phys.* 41 (4), 245–250.
- Simons, F.L., 1950. A stain for use in the microscopy of beaten fibers. *Tappi J.* 33, 312–314.
- Stilbs, P., 1987. Fourier transform pulsed-gradient spin-echo studies of molecular diffusion. *Prog. Nucl. Magn. Reson. Spectrosc.* 19, 1–45.
- Strange, J.H., Rahman, M., Smith, E.G., 1993. Characterization of porous solids by NMR. *Phys. Rev. Lett.* 71, 3589–3591.
- Suurnakki, A., Li, T.Q., Buchert, J., Tenkanen, M., Viikari, L., Vuorinen, T., Odberg, L., 1997. Effects of enzymic removal of xylan and glucomannan on the pore size distribution of kraft fibers. *Holzforschung* 51, 27–33.
- Tanaka, M., Ikesaka, M., Matsuno, R., Converse, A.O., 1988. Effect of pore size in substrate and diffusion of enzyme on hydrolysis of cellulosic materials with cellulases. *Biotechnol. Bioeng.* 32, 698–706.
- Tanner, J.E., Stejskal, E.O., 1968. Restricted self-diffusion of protons in colloidal systems by the pulsed-gradient, spin-echo method. *J. Chem. Phys.* 49, 1768–1777.
- Thompson, D.N., Chen, H.C., Grethlein, H.E., 1991. Comparison of pretreatment methods on the basis of available surface area. *Bioresour. Technol.* 39 (2), 155–163.
- Topgaard, D., Soederman, O., 2001. Diffusion of water absorbed in cellulose fibers studied with proton NMR. *Langmuir* 17, 2694–2702.
- Wang, Q.Q., He, Z., Zhu, Z., Zhang, Y.H.P., Ni, Y., Luo, X.L., Zhu, J.Y., 2012. Evaluations of cellulose accessibilities of lignocelluloses by solute exclusion and protein adsorption techniques. *Biotechnol. Bioeng.* 109, 381–389.
- White, A.R., Brown, R.M., 1981. Enzymatic hydrolysis of cellulose: Visual characterization of the process. *Proc. Natl. Acad. Sci. U.S.A.* 78, 1047–1051.
- Wiman, M., Dienes, D., Hansen, M.A.T., van, D.M.T., Zacchi, G., Liden, G., 2012. Cellulose accessibility determines the rate of enzymatic hydrolysis of steam-pretreated spruce. *Bioresour. Technol.* 126, 208–215.
- Yu, X., Atalla, R.H., 1998. A staining technique for evaluating the pore structure variations of microcrystalline cellulose powders. *Powder Technol.* 98, 135–138.